ELSEVIER

Journal of Nuclear Materials 294 (2001) 330–338

journal of nuclear materials

www.elsevier.nl/locate/jnucmat

# Effect of plastic shearing on damage and texture on Zircaloy-4 cladding tubes: experimental and numerical study

E. Girard [a,*], R. Guillén [a], P. Weisbecker [b], M. François [a]

[a] *Laboratoire d'Applications des Matériaux à la Mécanique, C.R.T.T. Boulevard de l'Université BP406, F-44602 Saint Nazaire cedex, France*

[b] *LSG2M Ecole Nationale Supérieure des Mines de Nancy Parc de Saurupt, F-54042 Nancy cedex, France*

Received 26 June 2000; accepted 8 December 2000

**Abstract**

Experimental evaluation of plastic shearing due to cold rolling Zircaloy-4 (Zy4) cladding tubes has been performed. An experiment design was used to evaluate the influence of three parameters on the shear stress: the feeding, the frequency of rolling steps, and the type of internal lubricant. Calculation and experimental analysis have shown a good correlation between a cumulative damage factor (CDF) and depth of defects in cold-pilgered tubes. The CDF depends strongly on the shear strain $\varepsilon_{zr}$. Texture simulations, using a visco-plastic self-consistent (VPSC) model, have been performed and compared with experimental pole figures (PF) obtained by X-ray diffraction. A very good agreement is obtained between experimental and simulated pole figures, specially in radial and axial directions (RD–AD) plane. Results have shown that a shear component in the strain rate tensor is necessary, and that the critical resolved shear stresses (CRSS) must be changed during pilgering to take into account the real pilgering conditions. 

## 1. Introduction

Zircaloy 4 (Zy4) is a zirconium alloy used for fuel cladding tubes in pressurised water nuclear reactors. As these tubes require a high quality level they are manufactured by cold pilgering (Mannesman 25 VMR). The tube is repeatedly rolled over a mandrel by two grooved dies. The grooved cross-section is basically a half circle which diameter evolves in an orthoradial direction with a parabolic law (between the initial and final tube diameters) [1]. The dies rotate around their axis while they move along the rolling axis (Fig. 1). A pinion-rack gearing system imposes synchronism. After each back and forth movement (stroke) of the dies, the raw tube is advanced by about 1 mm and turned by approximately 50°.

The plastic deformation and the subsequent texture formation that occur during cold pilgering of copper or Zy4 tubes, have been extensively studied [2–6]. However, experimental and theoretical works take into account a plastic strain tensor that is purely diagonal. This can be explained by the fact that the diagonal components can be obtained directly from dimensional measurements of the tube thickness and diameter before and after rolling. In fact, as we show in the present study, the strain path is much more complicated and the shear component in the rolling-radial direction is not negligible. Measurements of this shear strain were performed and the influence of pilgering parameters was studied with the help of experimental design techniques. The obtained values were then used as an input into a damage model. For that, the strain path undergone by a volume element of metal was described by the combined use of our measurements and a two-dimensional finite element method. The calculated damage was then compared with the defect rate found experimentally for various rolling conditions.

* Corresponding author. Fax: +33-2 40 17 26 18.

*E-mail address:* emmanuel.girard@lamm.univ-nantes.fr (E. Girard).

0022-3115/01/$ - see front matter 
PII: S0022-3115(00)00729-7

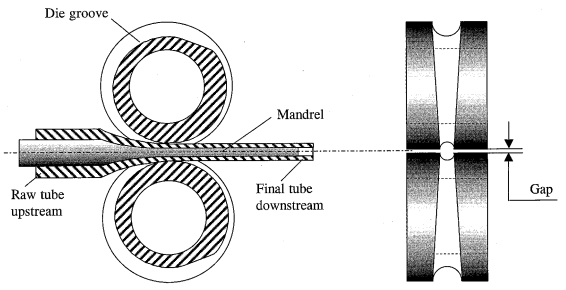


Fig. 1. Cold pilgering system with: the mandrel (tool inside the tube) and the dies (external tools with semicircular grooves).

The cold pilgering texture of zirconium alloys is well known [6,7]. Generally, studies were performed in cold-rolled sheets or rods with characteristic symmetrical basal {00.2} pole figures (PF). For Zy4 tubes, the {00.2} PFs show a twin-mode distribution of intensities in the RD–TD plane (RD: radial and TD: tangential sample directions) but an asymmetrical distribution of pole densities in RD–AD plane (AD: axial direction). This behaviour can be correlated to cold pilgering and to the shear strain produced in tubes.

Various attempts to explain the texture with micro-modelling of deformation mechanisms have been performed [3–6,8–10]. For instance, Lebensohn and Tomé [3,4] have proposed a self-consistent viscoplastic (VPSC) model, however the simulated PF did not fit accurately the experimental ones. In this work, we propose two improvements to reach a better agreement: a variation of the active strain systems during pilgering and a strain rate taking into account the shear component in the macroscopic plastic strain tensor.

## 2. Experimental strain analysis

### 2.1. Strain measurements

To observe the strain path in a copper tube during cold pilgering, Sheurer et al. [11] screwed pieces of rods in the thickness of the tube. We used this technique to analyse the last rolling pass of Zy4 cladding tubes [12]. The thickness of a raw tube (before cold-pilgering) was 1.8 mm and small cylinders of 0.4 mm diameter were inserted.

Several experiments have been performed:

- Rolling of raw parts containing 120 inserts aligned along the axis of the tube on four lines at 90°. The rolling was interrupted to observe the evolution of insert positions in the transition area between the raw tube and the finished one.
- Rolling of raw tubes with three inserts to compare different tool types and forming parameters.

The holes receiving the inserts were obtained by drilling with a high speed spindle (25 000 rpm) on a numeric machine tool. To manufacture the inserts, several materials were compared [1]. Cylinders made of tin, copper, mild steel and of a ternary Au–Ag–Cu alloy were used. The Au–Ag–Cu alloy was finally chosen because its mechanical behaviour is close to that of Zy4 and its contrast is suitable for subsequent analysis. After rolling, the angular position of two successive inserts varies from a few degrees (see Fig. 2) which gives rolling helices ranging from 90°/m to 600°/m according to the forming tool used.

The strains of the inserts were analysed by machining parallel planes in the depth of the tube. After the removal of each thin layer, the surface of the sample was photographed with magnifying lenses. A hole (0.4 mm of diameter) was drilled in the tube close to the insert to serve as a position and scaling reference (Fig. 3). The position and the shape of the insert in the thickness of the tube could then be reconstructed. The whole process of machining and photographing was automated using a numerical machine tool. These photographs allowed the

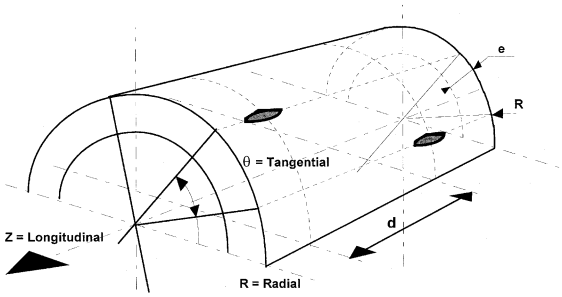


Fig. 2. Insert position with rolling helix.

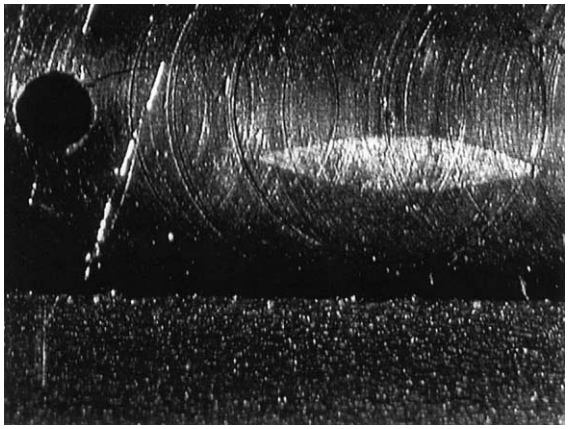

Fig. 3. Insert with hole drilling photograph.

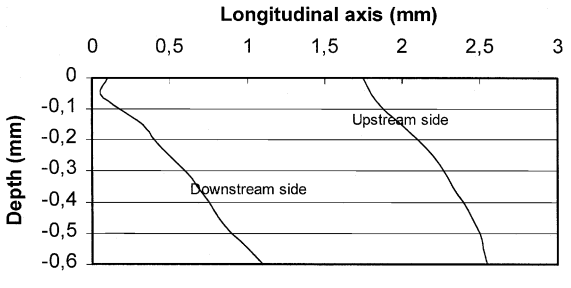


Fig. 4. Insert straining along longitudinal axis vs the depth on the tube (note the different scale on each axis).

values of axial and transverse strain components $\varepsilon_{zr}$ and $\varepsilon_{r\theta}$ to be obtained. The $\varepsilon_{\theta z}$ strain component, also called 'rolling helix' was observed macroscopically by measuring the angular position of several successive inserts along the axis of the tube. We found that the $\varepsilon_{r\theta}$ component is close to zero and we will neglect it in subsequent calculations. The strain $\varepsilon_{zr}$ was determined from the angular shift ($\gamma$) of the insert axis in the $(r, z)$ plane before and after deformation (Fig. 4).

To obtain $\gamma$, a straight line was fitted by least-square optimisation on the positions of the interface between the two materials for each photograph of an insert. $\varepsilon_{zr}$ can be approximated considering infinitesimal strains by $\varepsilon_{zr} = \gamma/2$. In standard rolling conditions, the measured strain component $\varepsilon_{\theta z}$ is negligible ($\sim$0.03) compared with $\varepsilon_{zr}$ ($\sim$0.45).

A high precision measurement (0.1 μm) of the profile in the transition area was performed by three-dimensional measuring machine. The presence of an upstream material wave was observed. It was noticed that this phenomenon increases when the tube thickness is decreased.

### 2.2. Parameters influencing the shear strain

To take into account $\varepsilon_{zr}$ in the analysis of cold pilgering, it is necessary to determine which parameters affect its value. A series of experiments were carried out to determine $\varepsilon_{zr}$ and the rolling efforts for several rolling tools and rolling conditions (friction, lubrication). For all of our experiments, the external lubricant is the one usually used in the process. The internal lubricants are commercial products for cold pilgering and are classified as:

- B the best.
- G good.
- M medium, even bad in some cases.

These three parameters were fed into a two-level experiment design [13]. The output parameters of the experiment design are the shear components $\varepsilon_{zr}$ and $\varepsilon_{\theta z}$.

Preliminary experiments enabled us to consider:

- two parameters related to the productivity of the rolling mill: (i) the feeding of the raw tube between two rolling steps, and (ii) the frequency of rolling steps which is related to the strain rate and dynamical efforts;
- one parameter influencing the tribological phenomena: the type of internal lubricant influencing the contact between the mandrel and the inner surface of the tube.

Three Au–Ag–Cu alloy inserts, separated by 10 mm, have been placed at 300 mm from the tip of a raw tube. To warm up the rolling mill, four raw tubes have been rolled before the specimen containing the inserts. To determine the measurement dispersion, we made one set of experiment three times and the repeatability of the experiments allowed us to find values of $\varepsilon_{zr}$: 0.47, 0.45 and 0.49. In order to determine the uncertainty, we have repeated an analysis on two inserts and by two different operators. The maximal deviation was about 3% and seemed adequate.

Results are summarised in Table 1. The 'lubricant' factor can be placed as a very influential parameter. An increase of 18% of the 'frequency' factor from fr1 to fr2 shows a weak lowering of the shear strain. The 'feeding' factor does not seem significant.

We can also conclude that the interactions are not significant. We can point out, however, a slight interaction between the lubricant and the feeding. We notice more particularly that if the lubrication is good, an increase in the feeding decreases the shear strain.

Moreover, the use of the best lubricant and the highest frequency (experiment number 8; Table 1) induce a decrease of 15% of the die separation with regard

Table 1
Experiment design showing the influence of frequency, lubricant and feeding to $\varepsilon_{zr}$ and $\varepsilon_{\theta z}$

| Experiment | Frequency | Lubricant | Feeding | $\varepsilon_{zr}$ | $\varepsilon_{\theta z}$ |
|---|---|---|---|---|---|
| 1 | fr 1 | M | fe 1 | 0.49 | 0.025 |
| 2 | fr 2 | M | fe 1 | 0.47 | 0.025 |
| 3 | fr 1 | B | fe 1 | 0.43 | 0.027 |
| 4 | fr 2 | B | fe 1 | 0.38 | 0.028 |
| 5 | fr 1 | M | fe 2 | 0.51 | 0.022 |
| 6 | fr 2 | M | fe 2 | 0.49 | 0.023 |
| 7 | fr 1 | B | fe 2 | 0.39 | 0.028 |
| 8 | fr 2 | B | fe 2 | 0.36 | 0.024 |

to the least favourable conditions (experiment number 5).

The best lubricant gives average $\varepsilon_{zr}$ value which is about 0.39 while the medium one gives $\varepsilon_{zr}$ about 0.49. It can be interpreted by saying that the shear strain depends mainly on the difference in friction conditions between the inner and the outer surfaces of the tube during pilgering. This interpretation was confirmed by two-dimensional Finite Element Method (Software FORGE2D®) of the rolling process: the strain $\varepsilon_{zr}$ decreases with the difference $\Delta f$ of friction coefficient between internal and external contacts [14]. An equivalent friction between internal and external surfaces tends to minimise this shearing.

## 3. Damage analysis during cold-pilgering

### 3.1. Presentation of the geometrical elements calculation

We observed the evolution of a material element, in the bottom of the groove, from the beginning of the reduction zone to the end of this zone. The calculation of the strain increments $\Delta\varepsilon_{rr}, \Delta\varepsilon_{\theta\theta}$ and $\Delta\varepsilon_{zz}$ proceeds from the tools geometry and the process kinematics. For the $i$th stroke of roll, the theoretical position of a particle is defined by the $(i-1)$th position and the product of the feeding by the elongation (that is to say, the ratio between the initial section and the local one).

We made the following assumptions:

- The geometry and radius of the tools are well known: the mandrel (tool inside the tube) and the rolls (external tools with semicircular grooves).
- Tools strains are considered as negligible except for the calculation of the contact length: this one has been calculated with Hitchcock's model [15].
- Equations of the mandrel movement are described by functions fitted on experimental results. The metal reduction zone (like a trumpet) and the mandrel move together because of the roll axial force component.
- The strained zone is provided by the process, with a 51° rotation after each roll stroke.
- Starting with an initial guess of the value of the gap (separation between matrix), the rolling efforts on the die have been calculated.
- Knowing the stiffness of the rolling mill (experimental results for well-known tools), a new value of the separation between the matrix was calculated. The model converges toward a value of the roll gap, which has been compared successfully with experimental values.

It has been shown [16] that the gap between the two rolls (Fig. 1) should be taken into account in the geometric description of rolling. We minimise the tube thickness variation by taking into account the roll gap as it was shown by a three-dimensional measurement of a transition.

### 3.2. Stress and strain calculation

The axial and orthoradial strain increments $(\Delta\varepsilon_{zz}, \Delta\varepsilon_{\theta\theta})$ between the $(i-1)$th and the $i$th step are deduced from

$$\Delta\varepsilon_{zz} = \ln\left[\frac{S_{(i-1)}}{S_{(i)}}\right] \quad \text{and} \quad \Delta\varepsilon_{\theta\theta} = -\ln\left[\frac{\overline{D}_{(i-1)}}{\overline{D}_{(i)}}\right] \tag{1}$$

with $\overline{D}_{(i)}$ the average diameter and $S_{(z)}$ the cross-section

The third strain increment is established from the two others according to the uncompressible plasticity hypothesis

$$\Delta\varepsilon_{rr} + \Delta\varepsilon_{zz} + \Delta\varepsilon_{\theta\theta} = 0. \tag{2}$$

The strain increments $\Delta\varepsilon_{zz}$ are considered as homogeneous around the cross-section. This strain analysis is completed by a calculation of the contact length between the die and the tube assuming elastic deformation of the die [17]. However, a purely elastic approach leads to an underestimation of the rolling efforts. It may be due to the observed material wave, which increases the contact length. This effect was taken into account in the model.

We use, in the first approximation, the Von Mises plastic flow rule for isotropic materials:

$$\begin{aligned}&(\sigma_{zz}-\sigma_{\theta\theta})^2 + (\sigma_{\theta\theta}-\sigma_{rr})^2 + (\sigma_{rr}-\sigma_{zz})^2 + 6(\sigma_{rz})^2\\ &\quad + 6(\sigma_{z\theta})^2 + 6(\sigma_{\theta r})^2 - 2\sigma_0^2 = 0,\end{aligned} \tag{3}$$

where $\sigma_0$ is the flow stress that depends mainly on the amount of cold work and secondarily on the temperature and the strain rate. The shape of this plastic flow criterion explains the importance of $\varepsilon_{zr}, \varepsilon_{r\theta}$ and $\varepsilon_{\theta z}$ strain measurements. As mentioned before, $\varepsilon_{\theta z}$ corresponds to the pilgering helix and leads to very weak strain values. The $\varepsilon_{r\theta}$ strain is negligible but $\varepsilon_{zr}$ is not: it is a very important parameter for the damage function calculation.

By the application of the Von Mises plastic flow rule for cancelling the terms that were found experimentally negligible, we obtain

$$\begin{aligned}\sigma_{\theta\theta}-\sigma_{zz} &= \frac{2}{3}\frac{\dot{\varepsilon}_{\theta\theta}-\dot{\varepsilon}_{zz}}{\dot{\bar{\varepsilon}}}\sigma_0\\ &= \sqrt{\frac{2}{3}}\frac{\Delta\varepsilon_{\theta\theta}-\Delta\varepsilon_{zz}}{\sqrt{\Delta\varepsilon_{\theta\theta}^2+\Delta\varepsilon_{zz}^2+\Delta\varepsilon_{rr}^2+2\Delta\varepsilon_{rz}^2}}\sigma_0,\\ \sigma_{rr}-\sigma_{zz} &= \frac{2}{3}\frac{\dot{\varepsilon}_{rr}-\dot{\varepsilon}_{zz}}{\dot{\bar{\varepsilon}}}\sigma_0\\ &= \sqrt{\frac{2}{3}}\frac{\Delta\varepsilon_{rr}-\Delta\varepsilon_{zz}}{\sqrt{\Delta\varepsilon_{\theta\theta}^2+\Delta\varepsilon_{zz}^2+\Delta\varepsilon_{rr}^2+2\Delta\varepsilon_{rz}^2}}\sigma_0,\\ \sigma_{rz} &= \frac{2}{3}\frac{\dot{\varepsilon}_{rz}}{\dot{\bar{\varepsilon}}}\sigma_0 = \sqrt{\frac{2}{3}}\frac{\Delta\varepsilon_{rz}}{\sqrt{\Delta\varepsilon_{\theta\theta}^2+\Delta\varepsilon_{zz}^2+\Delta\varepsilon_{rr}^2+2\Delta\varepsilon_{rz}^2}}\sigma_0.\end{aligned} \tag{4}$$

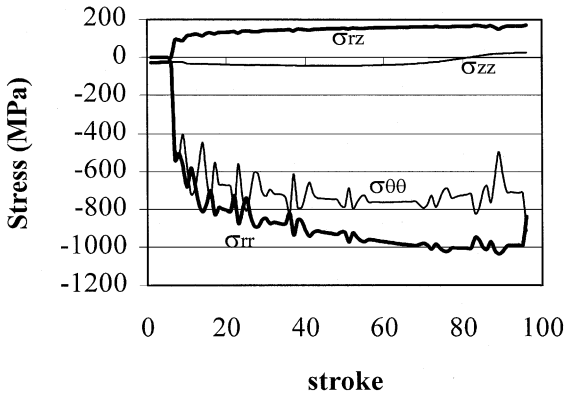


Fig. 5. Stress components calculation during the last cold pilgering pass of a Zy4 tube.

Calculation of the stress components $\sigma_{\theta\theta}, \sigma_{rr}$ and $\sigma_{rz}$ from this set of equations requires the knowledge of $\sigma_{zz}$, which was obtained by the slab method. This calculation allows one to determine $\sigma_{zz}$, the axial stress, according to the flow rule. A stress calculation applied to one particle at each stroke is presented in Fig. 5. From this figure, we can notice that $\sigma_{\theta\theta}$ and $\sigma_{rr}$ are highly compressive with mean values, respectively, about 800 and 1000 MPa. These stress variations are due to the rotation mechanism as well as the variation of the thickness of the tube around a cross-section.

Observations by three-dimensional metrology point out that this variation is overestimated because the calculation does not take into account the tools strain. The longitudinal stress $\sigma_{zz}$ induced by friction effects is small (about 25 MPa). The shear stress $\sigma_{rz}$ is positive and its mean value is about 150 MPa.

The stress components $\sigma_{r\theta}, \sigma_{\theta z}$ are negligible; therefore the complete stress tensor is obtained:

$$\bar{\bar{\sigma}} = \begin{bmatrix} \sigma_{\theta\theta} & 0 & 0 \\ 0 & \sigma_{rr} & \sigma_{rz} \\ 0 & \sigma_{rz} & \sigma_{zz} \end{bmatrix}. \tag{5}$$

### 3.3. The damage function

Our model was fed with the experimental values of $\varepsilon_{zr}$. In order to make the analysis easier, we only measure this shear component after total rolling of the tube. The damage determination is a way of foreseeing the material behaviour in relation to the different pilgering parameters. We were looking for an indicator to predict defects frequency.

The criterion introduced by Latham and Cockroft [18] and used in this work establishes the damage function from the principal stresses. Compressive stresses have a negligible effect on damage compared with tensile ones, therefore this criterion does not take them into account. The damage function is the sum of the product of the maximum tensile stress at each stroke. This function represents an indicator of the material state.

The cumulative damage function (CDF) is

$$\mathrm{CDF} = \sum_{\text{stroke}} \sigma^* \varepsilon_{\mathrm{eq}}$$

$$\text{with} \quad \varepsilon_{\mathrm{eq}} = \sqrt{\frac{2}{3}\left[\Delta\varepsilon_{\theta\theta}^2 + \Delta\varepsilon_{zz}^2 + \Delta\varepsilon_{rr}^2 + 2\Delta\varepsilon_{rz}^2\right]}, \tag{6}$$

$$\sigma^* = \max\left[\sigma_{\mathrm{I}}, \sigma_{\mathrm{II}}, \sigma_{\mathrm{III}}, 0\right],$$

$\sigma_{\mathrm{I}}, \sigma_{\mathrm{II}}, \sigma_{\mathrm{III}}$ are the principal stresses.

Fig. 6 and Table 2 show the comparison of the damage functions during the rolling.

To correlate the model results with defects occurrence, we pilgered about 2000 tubes (more than 8 km) with three tool geometries (U, V, W) and three qualities of lubricants commercially available (B, G, M) presented in Section 2.2.

The other factors remain constant. Damage analysis was performed to characterise some defects. The tubes were checked by ultrasonic inspection and rejected ones were visually inspected. Each defect has been visually proved and its depth has been measured by a macrographic section.

Three parameters were used to characterise the damage: (i) the $p\%$ factor which represents the percentage of tubes with defects. (ii) The $T_{\mathrm{d}}$ factor which represents the defects rate per kilometre of controlled tube. (iii) the maximum defect depth $D$.

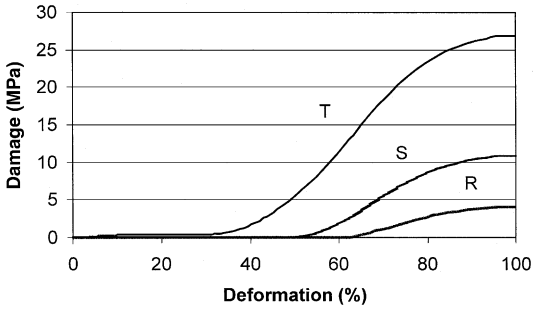


Fig. 6. Damage function in the reference conditions during the last cold pilgering pass of a Zy4 tube. The ($R$) curve represents the ideal rolling conditions with $\varepsilon_{zr} = 0.3$, the ($S$) curve, the hardest friction conditions with $\varepsilon_{zr} = 0.45$ and the ($T$) curve, $\varepsilon_{zr} = 0.6$.

Table 2
Strain $\varepsilon_{zr}$ and damage function calculated comparison in the reference conditions

| $\varepsilon_{zr}$ | 0.3 | 0.45 | 0.6 |
|---|---|---|---|
| Damage function (MPa or J/cm$^2$) | 4 | 11 | 27 |

Table 3
Defects and damage comparison for three tools and three lubricants during the last cold pilgering pass of a Zy4 tube[a]

| Experiment | | | Results | | | | |
|---|---|---|---|---|---|---|---|
| Die geometry | Lubricants | Number of tubes | $\varepsilon_{zr}$ | CDF ($10^6$ J/m$^3$) | $p$% | $T_d$ (km$^{-1}$) | $D$ (μm) |
| U | M | 438 | 0.81 | 64.2 | 3.42 | 154.5 | 80 |
| V | B | 429 | 0.44 | 10.3 | 1.4 | 4.4 | 35 |
| W | G | 635 | 0.47 | 7.9 | 1.4 | 4.9 | 40 |
| W | B | 509 | 0.33 | 2.9 | 0.4 | 0.87 | 25 |

[a] The factor $p$% represents the percentage of tubes with defects in comparison with all the tubes. The factor $T_d$ represents the defects rate per controlled tube kilometre. The third indicator of the defects severity is its maximum depth.

The analysis shows a good correlation between the damage factor CDF, defects presence and depth. The number of defects is not very large but large enough to be representative of the damage. Table 3 represents the defects frequency in relation to their depth and the tools that were used. We can see that the tool geometry has a very strong influence on the damage. However, for a given geometry, the lubricant (the friction conditions), is very important. The CDF, as well as the shear strain are good indicators of damage occurrency and severity. In particular, effort in reducing the damage rate should be aimed at reducing the shear strain, i.e. improving the friction conditions at the interface tool tube rather than focusing on the reduction rate or the $Q_p$ factor.

The calculated damage function must be considered as an indicator. This parameter depends strongly on the shear strain $\varepsilon_{zr}$. This strain depends on pilgering conditions and more particularly on friction conditions. A model has been thought to determine $\varepsilon_{zr}$ to avoid providing an experimental measurement.

## 4. Crystalline texture simulation

In order to analyse the different active deformation modes present in each grain, strain texture simulation was performed from a VPSC model [3,4]. Each grain is treated as an inhomogeneity embedded in the homogeneous effective medium represented by the polycrystal, with the condition that the average of stress and strain rate over all the grains must be consistent with the equivalent macroscopic magnitudes.

The VPSC model combined with a volume fraction transfer (VFT) scheme, developed by Lebensohn and Tomé [4], allow a particular treatment of the re-orientation by twinning, which could be present in the manufacturing of Zy4 tubes.

### 4.1. Experimental

The analysis was performed for the last cold pilgering pass. For experimental PFs the recrystallised tubes were thinned by chemical etching and unrolled to form a flat sample. Average grain size was about 20 μm. Incomplete PFs were performed with an open Eulerian cradle using Cu Kα radiation. Recorded peaks were obtained with an INEL position-sensitive detector. The maximal tilt value was $\psi = 75°$, the azimuth angle varied from 0° to 360° in steps of 5°. For each experimental measurement direction we obtained a diffraction spectrum which was adjusted using a non-linear least-squares analysis assuming a pseudo-Voigt peak profile. The ODF calculation was carried out with the spherical harmonic method, using experimental PFs (00.2), (10.1), (11.0) and (10.3). It gives for each orientation in the Euler space, the corresponding ODF intensity $f(\Omega)$.

### 4.2. Simulation

Using a VPSC model, for each orientation $\Omega(\phi_1, \phi, \phi_2)$ we assign the weight $w$ corresponding to $dV(\Omega)/V$ fraction as the initial parameter of the simulation. The global strain matrix is defined according to Eqs. (1) and (2). The total equivalent Von Mises strain is equal to 1.75. For the used VPSC model, the initial inclusion is assumed spherical. The texture calculation of cold pilgering Zy4 tubes after rolling has been performed by Lebensohn et al. [6]. They have taken into account the critical resolved shear stresses (CRSS) of three strain systems: prismatic slip pr$\langle a\rangle$, tensile twinning ttw and pyramidal slip pyr$\langle c + a\rangle$. They have obtained an acceptable agreement between measured and predicted textures but some discrepancies remained, mainly in RD–AD plane. This brings us to change critical values during pilgering assuming important changes of deformation systems because of the large strain. This method has been used by Serghat et al. [10] and Philippe et al. [19] who simulated texture of cold rolling Zy4 sheets subjected to large strains. In first approximation, we have arbitrarily divided the simulation: from 0% to 50%, from 50% to 100%, from 100% to 150% and from 150% to 175% equivalent strain. The CRSS have been then selected in order to keep a relative activity of the prismatic slip pr$\langle a\rangle$ up to 90%. We also have

Table 4
Deformation system activity during the last cold pilgering pass of a Zy4 tube, arbitrarily divided into four equivalent strain steps between 0%, 50%, 100%, 150% and 175%[a]

| Simulation | 0–50% | | 50–100% | | 100– 150% | | 150–175% | |
|---|---|---|---|---|---|---|---|---|
| | $\tau c$ | Activity | $\tau c$ | Activity | $\tau c$ | Activity | $\tau c$ | Activity |
| pr$\langle a\rangle$ | 1 | 96.3 | 1 | 98.9 | 1 | 100 | 1 | 100 |
| pyr$\langle c+a\rangle$ | 2.5 | 2.1 | 3 | 1.1 | 4 | 0 | 4 | 0 |
| ttw1 | 1.5 | 1.6 | 1.5 | 0 | 1.5 | 0 | 1.5 | 0 |

[a] pr$\langle a\rangle$: prismatic slip, pyr$\langle c+a\rangle$: pyramidal slip, ttw1: tensile twinning.

imposed a gradual hardening of the other slipping systems (Table 4).

The obtained texture looks like the experimental one and we clearly see the basal poles preferentially oriented at 30–40° from RD in the RD–TD plane. But there is no reinforcement in the RD–AD plane, maybe due to the quite rough discretisation step (10°) used in calculation.

These results induce the following observations (see Fig. 7(a)):

- The pr$\langle a\rangle$ slip produces the rotation of 30° along $\phi_2$ (from 30° at the initial state to 0° at the final one).
- The pyramidal pyr$\langle c+a\rangle$ slip creates the reinforcement observed in the RD–TD plane because, on the one hand, pr$\langle a\rangle$ does not reorientate the $\vec{c}$ axis and, on the other hand, the reinforcement is observed without tensile twinning.
- The prismatic slip activation cannot explain by itself the global material strain.

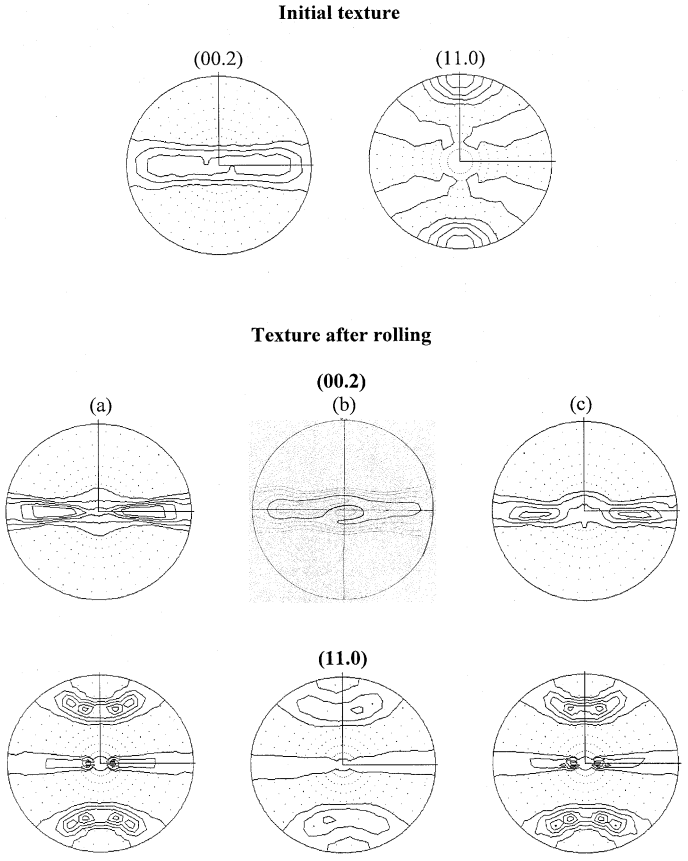


Fig. 7. PF (00.2) and (11.0) obtained by simulation of the last cold pilgering pass: (a) arbitrarily divided into four equivalent strain steps between 0%, 50%, 100%, 150% and 175% and (c) introducing a shearing $\varepsilon_{zr}$ up to 100%. PF obtained by ODF calculation (b) are showing to compare simulation results.

Table 5
Strain mode activity during the last cold pilgering pass of the ZY4 tube, arbitrarily divided into four equivalent strain steps between 0%, 50%, 100%, 150% and 175% and a shearing $\varepsilon_{rx}$ applied up to 100%

| Simulation | 0–50% | | 50–100% | | 100–150% | | 150–175% | |
|---|---|---|---|---|---|---|---|---|
| | $\tau c$ | Activity | $\tau c$ | Activity | $\tau c$ | Activity | $\tau c$ | Activity |
| pr$\langle a \rangle$ | 1 | 92.7 | 1 | 94.8 | 1 | 99.8 | 1 | 100 |
| pyr$\langle c+a \rangle$ | 2.3 | 7.1 | 2.5 | 5.0 | 4 | 0 | 4 | 0 |
| ttw1 | 1.25 | 0.2 | 1.25 | 0.2 | 1.25 | 0.2 | 1.25 | 0 |

- The weak activation of the tensile twinning is normal because it reorientates preferentially the grains which $\vec{c}$ axis is close to the AD.

From the results of the first part, we can analyse the parameters that were not taken into account in the simulation:

- In opposition to the assumption made, the die pressure on the tube is not homogeneous and the strain of one volume element varies continuously during one stroke.
- The pilgering wave has not been considered [1].
- The shearing $\varepsilon_{zr}$ variation cannot be negligible in the thickness.

So we have introduced a component $\varepsilon_{zr}$ in the strain rate tensor to come closer to the real pilgering conditions ($\varepsilon_{\theta z}$ is considered negligible and having no influence on texture). It is supposed that shearing occurs especially at the beginning of the strain (up to $\varepsilon_{\text{eq}} = 100\%$). Thus the strain rate tensor becomes

$$\dot{\varepsilon} = \begin{pmatrix} -0.34 & 0 & 0 \\ 0 & -0.66 & 0.3 \\ 0 & 0.3 & 1.0 \end{pmatrix}. \tag{7}$$

These simulation results are described in Table 5 and Fig. 7(c).

The simulated texture is very close to the experimental one because in the RD–AD plane, we find the same asymmetry that seems to be due to the pyr$\langle c+a \rangle$ slip when the tube is submitted to the shear strain mentioned above.

The VPSC model allows one to confirm that most of deformation is accommodated through prismatic $\langle a \rangle$ slip. However, the pyr$\langle c+a \rangle$ and tensile twinning ttw1 modes have no vanished activities, and they vary in relation to the equivalent strain degree. For zirconium alloys, the activity of pyr$\langle c+a \rangle$ and twinning tw1 systems for low deformations has been reported by other authors [19–21]. Besides, it is proved that the shear component plays an important role in the first steps of cold pilgering and it must be take into account for more accurate calculations and a better agreement with experimental textures. New simulations are in progress to take into account the mechanical hardening in the cold rolling process.

## 5. Conclusion

Measurements of the shear strain of Zy4 tubes during cold pilgering have been performed with inserts. An experiment design showed that it mainly depends on the friction difference between internal and external contacts with the tools. A damage model derived from Lathan and Cockroft was propos4 take into account this shear strain. It gives good correlation with experimental damage measurements and with tool profile changes.

A VPSC model allowed one to show that the prismatic mode is the most active system but that the pyramidal $\langle c+a \rangle$ slip and tensile twinning do have a role that varies with the strain degree. The experimental values of the shear strain have been taken into account in the model and led to more accurate description of experimental textures.

## References

[1] E. Girard, doctoral thesis, Univ. de Nantes, France, 1993.
[2] H. Yoshida, T. Matsui, T. Otani, K. Mandai, J. CIRP 24 (1975) 191.
[3] R. Lebensohn, C.N. Tomé, Acta Metall. Mater. 41 (1993) 2611.
[4] R. Lebensohn, C.N. Tomé, Mater. Sci. Eng. A 175 (1994) 71.
[5] P.A. Turner, C.N. Tomé, Acta Metall. Mater. 42 (1994) 4143.
[6] R. Lebensohn, M.I. Gonzalès, C.N. Tomé, A. Pochettino, J. Nucl. Mater. 229 (1996) 57.
[7] E. Tenckhoff, ASTM STP 976 (1988) 1.
[8] H. Francillette, B. Bacroix, M. Gasperini, J.L. Béchade, Acta Mater. 46 (1998) 4131.
[9] J.J. Fundenberger, M.J. Philippe, F. Wagner, C. Esling, Acta Mater. 45 (1997) 4041.
[10] M. Serghat, M.J. Philippe, C. Esling, Journées d'Etudes sur le Zirconium, Les Editions de Physique, 1995, p. 67.
[11] W. Sheurer, P. Grüner, A. Pomp, Stahl Eisen 71 (1951) 760.
[12] J.L. Aubin, E. Girard, P. Montmitonnet, in: 10th International Symposium of Zirconium, ASTM, Baltimore, MD, 1993, p. 245.
[13] W.J. Diamond. Practical Experiment Designs, Van Nostrand Reinhold, New York, 1989, p. 89 (Chapter 6).

[14] S. Mulot, doctoral thesis, Ecole Nationale Supérieure des Mines de Paris, France, 1997.
[15] J.H. Hitchcock, Report ASME res. Commitee, 1935.
[16] M. Furugen, C. Hayachi, J. Met. Working Technol. 10 (1984) 273.
[17] F.W. Neumann, E. Siebel, Stahl Eisen 74 (1954) 133.
[18] D.J. Latham, M.G. Cockroft, J. Inst. Met. 96 (1968).
[19] M.J. Philippe, M. Serghat, P. Van Houtte, C. Esling, Acta Metall. Mater. 43 (1995) 1619.
[20] H. Francillette, B. Bacroix, M. Gasperini, J.L. Béchade, Mater. Sci. Eng. A 234–236 (1997) 974.
[21] P.A. Turner, N. Christodoulou, C. Tomé, Int. J. Plast. 3 (1995) 251.